Global Scientific JOURNALS

GSJ: Volume 11, Issue 4, April 2023, Online: ISSN 2320-9186
www.globalscientificjournal.com

IMPACT OF DUAL DIRECT INJECTION ON NITROGEN OXIDE FORMATION IN GDI ENGINE AT EARLY INJECTION MODE

Felix Zator Tembile and Philip Baidoo

fztembile@aamusted.edu.gh and mypennich@yahoo.com

corresponding author: Philip Baidoo, Email: mypennich@yahoo.com,

Phone Number: +233 (0) 244162783, Country: Ghana

Akenten Appiah-Menka University of Skills Training and Entrepreneurial Development

Kumasi

ABSTRACT

Late injection for a stratified charge could realize Gasoline Direct Injection (GDI) engine's full potential in terms of fuel economy and emissions. A current study shows that lean mixture creation in the combustion chamber causes misfire, hydrocarbon, and NOx emissions potentially weakening the engine's advantage over the port fuel injection (PFI) engines. This work explores the impact of dual direct injection on NOx formation in a GDI engine at early injection mode. The 2021 ANSYS Design modeler was used for the geometry design, and meshing, and employed ANSYS Fluent for simulation, and numerical analysis. Post-combustion mass fraction of nitrogen and its corresponding oxides of nitrogen content in the combustion chamber were about ten times lower in the early injection mode of the dual direct injection engine in comparison to the same in the late injection mode. The results suggest that dual direct injection enhances progressive cooling of the charge and in-cylinder temperature for the mitigation of NOx formation.

KEYWORDS: Gasoline Direct Injection; NOx Formation; Port Fuel Injection; ANSYS Fluent; Combustion Chamber

1. INTRODUCTION

Greenhouse gas emissions which are setbacks of the gasoline direct injection engines have the potential to affect human health in several ways. Franchini and Mannuci (2015) emphasized that the ways by which these gases affect human health includes increased in the frequency of heat waves, weather events such as hurricanes, cyclones and drought. In an attempt to solve these setbacks exhaust gas recirculation (EGR), common rail system and direct injection has been introduced. Over the last three decades, limit values have been significantly decreased, and more pollutant species have been monitored. For example, the NOx threshold in Euro 5 and 6 has diminished by 60%, from 0.15 g/km in Euro 3 (European Commission,1998) to 0.06 g/km (European Commission,2012). Direct injection (DI) systems also came with its challenges that in Awad (2020) concluded in his work that direct injection engines would need to use gasoline particulate filters to comply with the recent emission laws. Meanwhile, DI engines inject fuel straight forwardly into every chamber, thus, eliminating time lag and improving transient response to result in evaporation of fuel inside the combustion domain for its cooling effect.

Spark ignition engines benefit from this cooling effect in a variety of ways, including volumetric efficiency, decreased knock propensity, bigger compression ratios, greater turbo charging, higher thermal efficiency and chiefly, fewer NOx emissions. In sum, the cooling effect of directly injected charge could result in fewer NOx emissions. Furthermore, the cooling impact of the directly injected fuel might be amplified if the fuels of higher vaporization enthalpies are used. In general, there are two types of Gasoline Direct Injection (GDI) engines, each with its own injection strategy: early injection for homogenous charge and late injection for stratified charge. It is suggested that the latter could realize the GDI engine's full potential in terms of fuel economy and emissions (Kalghatgi, 2019). Despite the fact that the GDI engine produces more power at part load, current study shows that the lean mixture creation in the combustion chamber might cause misfires and unburned hydrocarbon emissions, potentially weakening the engine's advantage over the PFI engine. Again, Investigation into the Comparisons of Exhaust Emissions through Catalytic Converters Installed during a similar experimental work done influenced the Exhaust system (Baidoo Philip et al 2022). As a result, the quality of mixture creation in the GDI engine with late injection should be improved to offset the influence of potential downsides of lean mixture formation. To add to that, the time for gasoline to combine with air in GDI engines with late injection is restricted (Anenberg, Miller, Henze, & Minjares, 2019). From this, late injection GDI engine, as well as the mixture formation and fuel atomization processes that lead to fuel vaporization and combustion of the air-fuel combination, has become a study focus. According to Price et al. (2007) directly injected fuel's impact may be measured in variety of ways. The researcher therefore seeks to explore the impact of dual direct injection on nitrogen oxide formation in a GDI engine at early injection mode.

2.0 METHODOLOGY

2.1 Numerical Method

Chemical species of gasoline-air combustion are examined at both early and late injection modes using eddy-dissipation model in ANSYS fluent. physical models; heat transfer is enabled by the

energy equation, standard k-epsilon turbulence model is selected in the viscous model and chemical species transport and reaction enabled by selecting the species transport model. A generalized eddy-dissipation model to analyze the gasoline-air combustion system was enabled. The combustion was modeled using a one-step reaction mechanism, assuming complete conversion of the fuel to CO_2 and H_2O. The reaction equation is $C_8H_{18} + 12.5\ (O_2 + 3.76\ N_2) \rightarrow 8\ CO_2 + 9H_2O + 47\ N_2$. This reaction is defined in terms of stoichiometric coefficients, formation enthalpies, and parameters that control the reaction rate. The reaction rate is determined assuming that turbulent mixing is the rate-limiting process, with the turbulence-chemistry interaction modeled using the eddy-dissipation model. Default setting for the mixture is modified by enabling the gas law. By default, the mixture material uses constant properties. These constant property assumptions are retained, allowing only the mixture density to vary with temperature and composition. The influence of variable property inputs on the combustion prediction are examined.

2.2 Geometry of the Combustion Chamber

Table 1 Main Technical Parameters of the Engine (The engine is designed using ANSYS 2021 Software).

Engine	**Spark ignition, four cylinders, dual-injection**
Compression	9.6:1
Displacement	1.984L
Cylinder Bore and stroke	82.5 mm x 92.8mm
Maximum Power	137KW (5000rpm)
Maximum Torque	320Nm(1600-4000rpm)

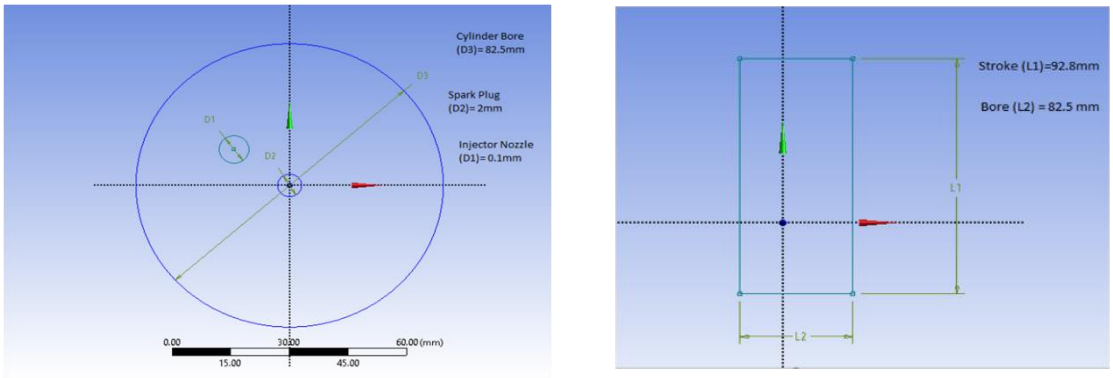

Figure 1. Dimension of cylinder bore and stroke

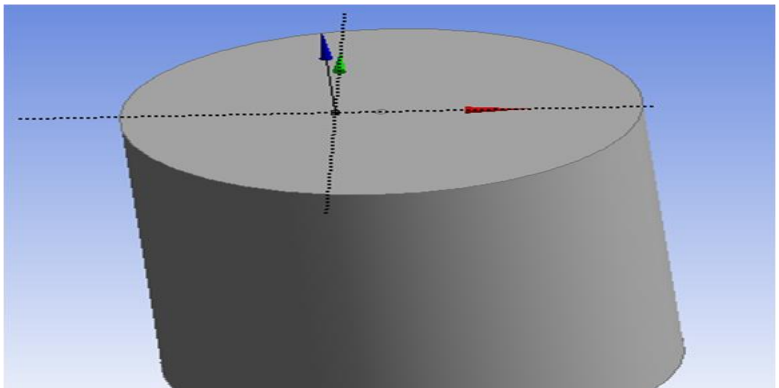

Figure 2. 3D geometry of a computational domain with piston at BDC.

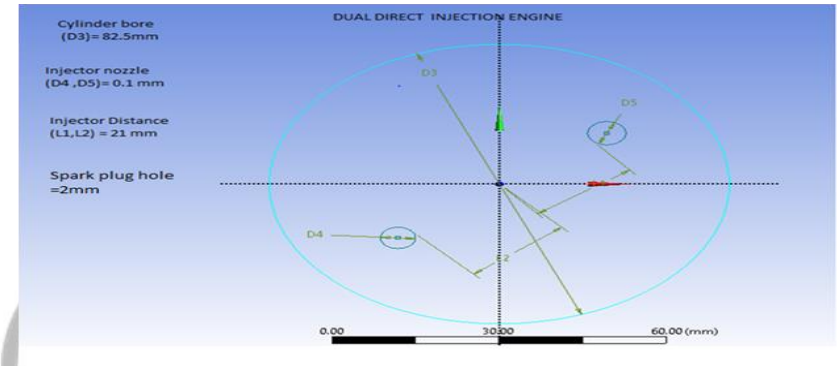

Figure 3. Dimensions of the dual direct injection model

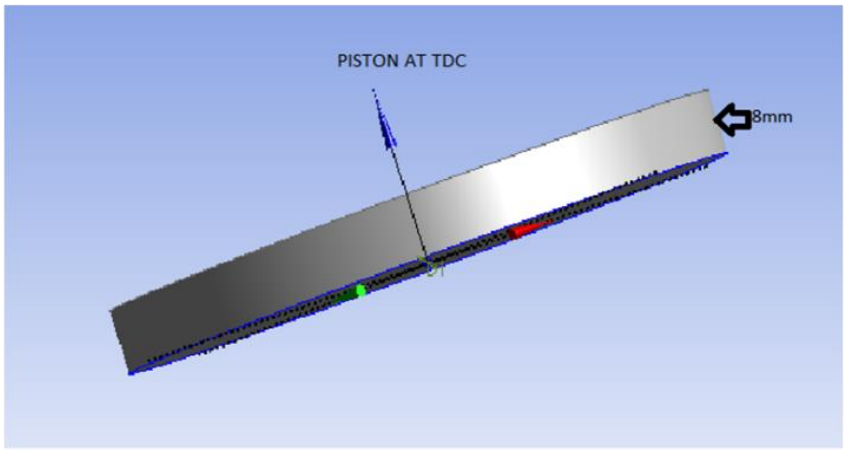

Figure 4. 3D geometry of the computational domain with piston at TDC

2.3 Meshing

Meshing is a necessary piece of the engineering simulation process where complex geometry is partitioned into straightforward components that can be utilized as discrete approximations of the

bigger area. The mesh impacts the precision, convergence and speed of the simulation. In the case of meshing being precise, then, at that point the results are additionally expected to be practical. Whoever, effective meshing has a great influence in simulation, referenced to comparative work done of experimental and simulation, the work corresponded same (Baidoo Philip, 2020). The present geometry is a mesh in ANSYS Software for the GDI and Dual injection engines.

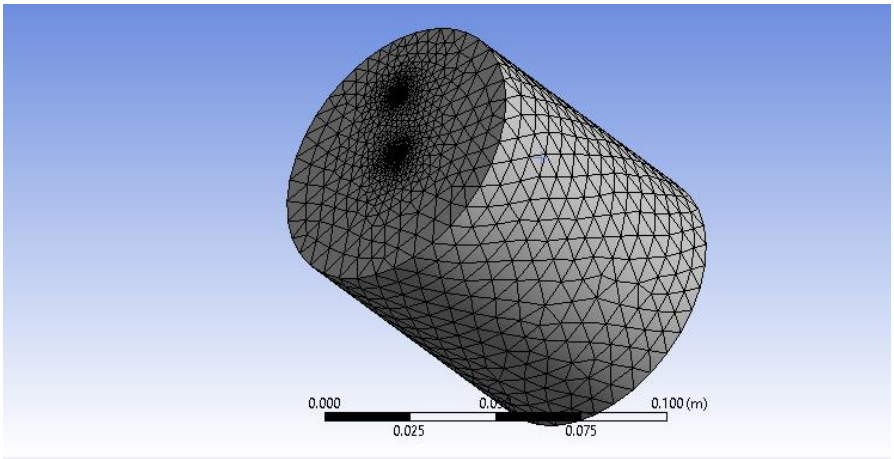

Figure 5. Mesh of cylinder with single direct injector at BDC

This is an automatic mesh of a single injector computational domain at the bottom dead centre. The mesh has 6694 nodes and 34806 elements.

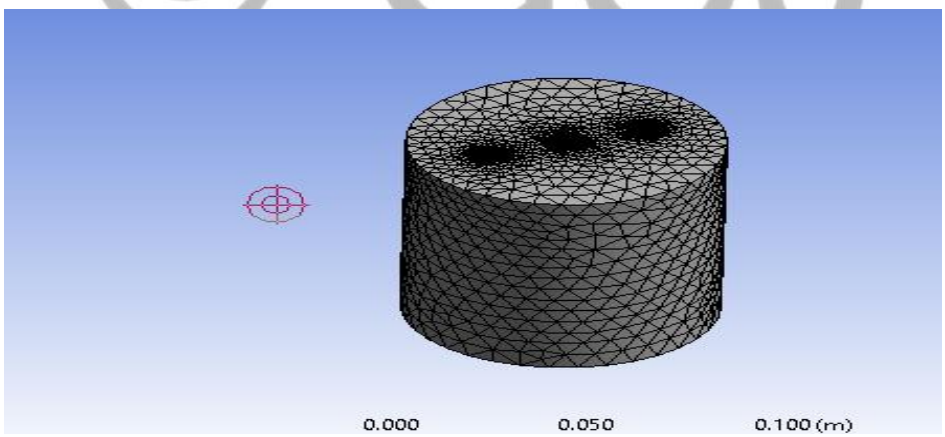

Figure 6. Mesh of cylinder with dual direct injector at BDC

This is an automatic mesh of a dual direct injector computational domain at bottom dead centre. The mesh has 9272 nodes and 48752 elements.

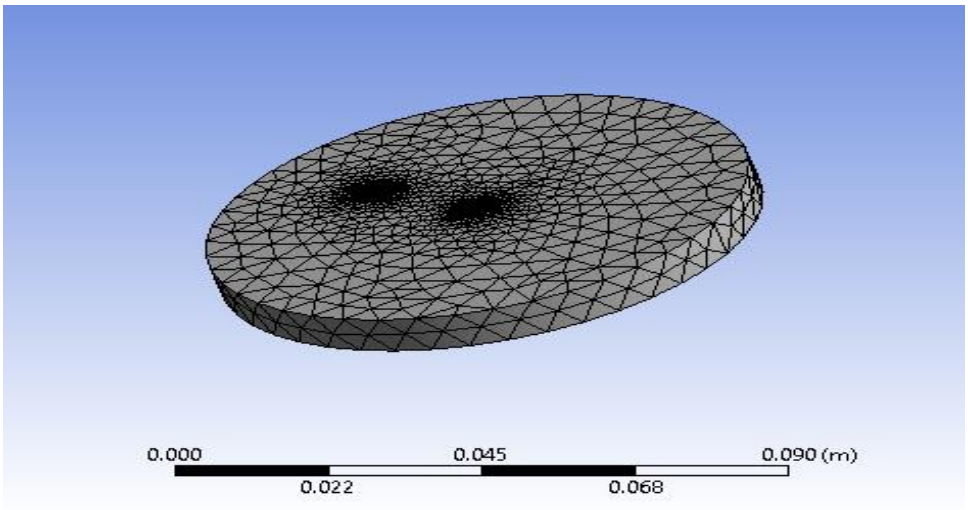

Figure 7. Mesh of cylinder with single direct injector at TDC

This is an automatic mesh of a single direct injector computational domain with the piston at top dead centre. The mesh has 4885 nodes and 24589 elements.

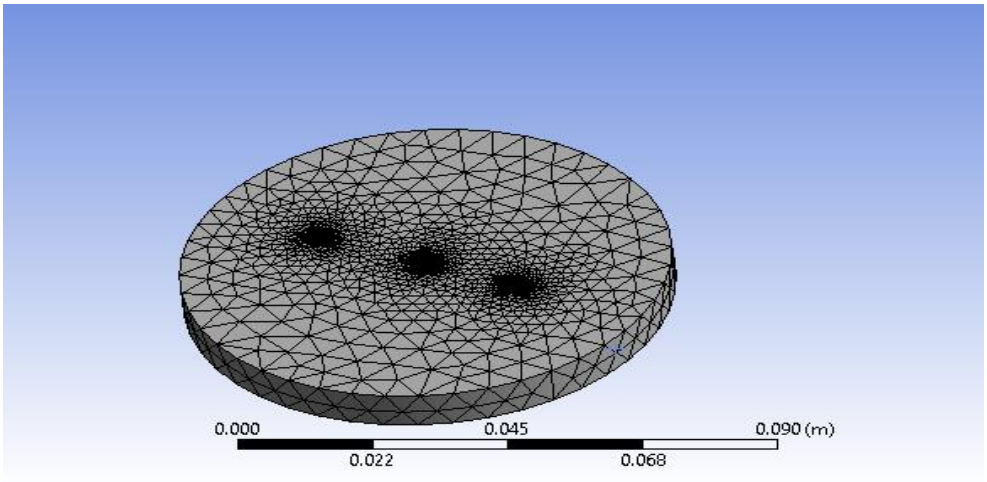

Figure 8. Mesh of cylinder with dual direct injector at TDC

This is an automatic mesh of a dual direct injector computational domain at top dead centre. The mesh has element of 38073 and 7412 nodes having the element size to be 5.8473e-003 m.

2.4 Procedural Approach

Fluent launcher was also used to start the 3D version of ANSYS FLUENT with double precision enabled for combustion and post combustion analysis. The imported mesh is checked to ensure that the reported minimum volume is positive. Heat transfer is activated by enabling the energy equation in the model. standard k-epsilon turbulence model is also selected from the viscous model and finally, chemical species transport and reaction model is enabled in the species model. Eddy-

dissipation in the turbulence chemistry interaction is enabled to compute the rate of reaction under the assumption that chemical kinetics are fast as compared to the rate at which reactants are mixed by eddies. Gasoline-air is selected in the species model and 1000J/Kg-K is entered for a constant specific heat value in the Cp drop down. Intensity and hydraulic diameter are selected for specification method for the air inlet zone. velocity magnitude of air is set to 0.5m/s, default setting for turbulence intensity is retained at 10% and the hydraulic diameter set to 0.44m, the air temperature at 300K and 0.23 for O_2 species mass fraction. Intensity and hydraulic diameter are also selected for specification method for fuel inlet zone. Fuel velocity magnitude of air is set to 80m/s, default setting for turbulence intensity is retained at 10% and the hydraulic diameter set to 0.01m, the air temperature at 300K and 1 for $C_{16}H_{29}$ species mass fraction. The gauge pressure value for the pressure outlet is 0Pa. intensity and hydraulic diameter is selected for its specification method. Backflow turbulent intensity is set to 10% in the backflow diameter of 0.45m at a backflow total temperature of 300K and 0.23 species mass fraction for O_2. Temperature of 300K is selected for the thermal condition of the outer wall. The solution is first done with constant heat capacity with the default solution parameters retained in the solution methods. Under -relaxation factors for the species were set to 0.95 since the default parameters in ANSYS FLUENT are set to high value. Plotting of residual during calculation is enabled in the monitor. Field variables are initialized by computing from selecting all-zone from the drop-down list and the variables are initialized. Calculation was started by requesting 500 iterations. For solution with varying heat capacity, composition dependence of the specific heat is enabled by selecting mixing law from Cp drop down in the properties group box mixture selection. This sis to ensure that specific heat of the mixture is based on a local mass-fraction weighted average of all the species. Temperature dependence of specific heat is enabled for CO_2, O_2, $C_{16}H_{29}$, and H_2O by ensuring piecewise polynomial in the Cp drop down is selected. 500 more iterations are requested and calculations ran.

2.5 Species Transport Model

The governing transport equations, including mass, momentum, energy, and species conservations, were solved numerically under steady-state and turbulent flow conditions with a set of finite-rate reaction kinetics and eddy-dissipation rates.

In this study the Navier-Stokes equations are considered as

$$\nabla.(\vec{\rho}\vec{v}) = -\nabla p + .\rightarrow(\bar{\bar{\tau}} +)Si \quad (1.1)$$

Where the stress tensor $\bar{\bar{\tau}}$ is given by

$$\bar{\bar{\tau}} = \mu\left[(\Delta\,\vec{v} + \nabla\vec{v}^{T}) - \frac{2}{3}\right]\nabla.\vec{v}I \quad (1.2)$$

and the porous media source term, $S_{i,}$ is expressed as

$$S_{i,} = -\left(\frac{\mu}{\alpha}\,V_i + C_2\frac{1}{2}\rho\,|V_i\,|V_i\right) \quad (1.3)$$

The permeability, α, and inertial loss coefficient, $C_{2,}$ can identified as

$$\alpha = \frac{D_p^2}{150}\frac{\varphi^3}{(1-\varphi)^2} \; and \; C_2 = \frac{3.5}{D_p}\frac{(1-\varphi)}{\varphi^3} \tag{1.4}$$

The continuity equation is expressed as follows:

$$\nabla.(p\vec{v}) = 0 \tag{1.5}$$

The energy transport equation is solved with the modification of the conduction flux, using the effective conductivity, including turbulent contribution, as

$$\nabla.\left(\vec{v}(ph+p)\right) = \nabla.\left(k_{eff}\nabla T - \sum_j h_j\vec{J_j}\right) + S_h \tag{1.6}$$

Where the sensible enthalpy, *h*, and the effective thermal conductivity,$k_{eff,}$ are defined as

$$h = \sum_j Y_j h_j \; and \; k_{eff} = \alpha c_p \mu_{eff} \tag{1.7}$$

Similarly, the transportation of species is expressed as

$$\nabla.(p\vec{v}Y_i) = -\nabla.\left(-\left(pD_{i,m} + \frac{\mu_t}{Sc_t}\right)\nabla Y_i\right) + R_i \tag{1.8}$$

Where *i* denotes the CO, CO_2, O_2, CH_4, H_2, H_2O, C, and N_2 species, R_i is the net rate of production of the species *i* by chemical reactions, and Sc_t is the turbulent Schmidt number, which is a ratio of the turbulent viscosity to the eddy diffusivity. Because the flow was turbulent, a Reynolds-averaging technique was employed to derive the Reynolds-averaged Navier-Stokes (RANS) equations (Eqs. (1.1) – (1.7)). Subsequently, the additional Reynolds stresses, representing the effects of turbulence, introduced in Eq. (1.1), were modeled using the Boussinesq hypothesis approach. It relates the Reynolds stresses to turbulent viscosity, μ_t, which is a function of the turbulence kinetic energy, k, and turbulence dissipation rate, ε. Subsequently, the two additional transport equations for *k* and *ε* were solved simultaneously using the RANS equations. The RNG-based k-ε turbulence model, using a mathematical technique called a renormalization group method, was more accurate and reliable, and can be expressed as

$$\frac{\partial}{\partial x_i}(pku_i) = \frac{\partial}{ax_j}\left(\alpha_k\mu_{eff}\frac{\partial k}{\partial x_j}\right)\frac{\partial u_j}{\partial x_i} + G_k - \rho\varepsilon \tag{1.9}$$

$$\frac{\partial}{\partial x_i}(p\varepsilon u_i) = \frac{\partial}{ax_j}\left(\alpha_\varepsilon\mu_{eff}\frac{\partial \varepsilon}{\partial x_j}\right) + C_{1\varepsilon}\frac{\varepsilon}{k}(Gk) - C_{2\varepsilon}\rho\frac{\varepsilon^2}{k} - R_\varepsilon \tag{1.10}$$

The right-hand terms represent the diffusion, generation, and destruction, respectively. In these equations, μ_{eff} is the turbulent or eddy viscosity. The model constants $C_{1\varepsilon}$ and$C_{2\varepsilon}$ in Eq. (1.10) had values derived analytically using RNG theory. These values are $C_{1\varepsilon}$ = 1.42, $C_{2\varepsilon}$ = 1.68.

3.0 RESULTS AND DISCUSSIONS

3.1 Mass Fraction of Nitrogen (N_2) at Late injection mode (Piston at BDC)

Figure 9. Contours plot of Nitrogen Mass Fraction of Single GDI

The mass fraction of Nitrogen gas in the cylinder before the start of combustion was at its highest of 7.70e-01. The quantity of Nitrogen reacts during combustion leaving burnt mixture to have a minimum mass of Nitrogen molecules. From fig 7.1, the minimum mass fraction recorded during combustion is 3.21e-01 and the average mass fraction of oxygen gas that could be present in the course of combustion is 5.46e-01.

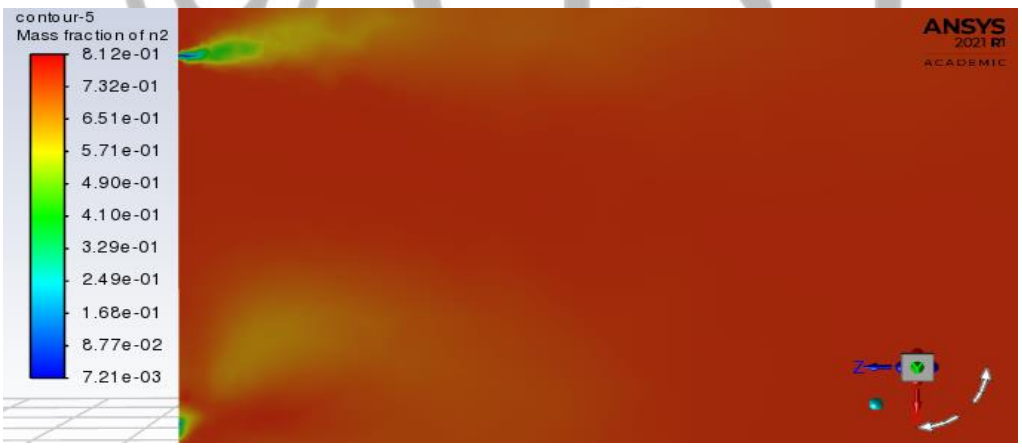

Figure 10. Contours plot of Nitrogen Mass Fraction of dual GDI

At the start of combustion, the mass fraction of Nitrogen is at its peak of 8.12e-01. The burning mixture has the minimum mass fraction of Nitrogen of 7.21e-03 since it reacts with oxygen and octane. As the flame propagates into the unburnt mixture, the Nitrogen molecules further reacts in the burning process to an average of 4.1e-01.

3.2 Mass fraction of Nitrogen (N_2) at Early injection mode (Piston at TDC)

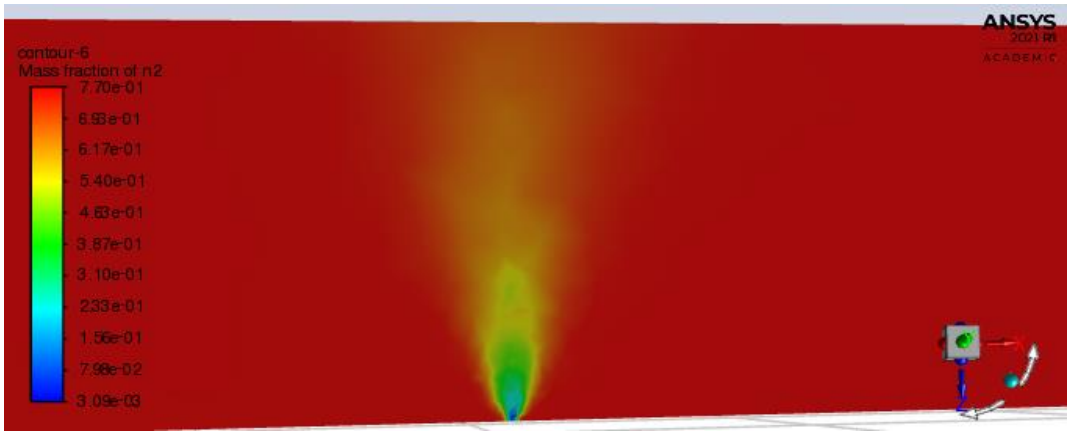

Figure 11. Contours plot of Nitrogen Mass Fraction of Single GDI

At the start of combustion, the mass fraction of Nitrogen is at its peak of 7.70e-01. The burning mixture has the minimum mass fraction of Nitrogen of 3.09e-03 since it reacts with oxygen and octane. As the flame propagates into the unburnt mixture, the Nitrogen molecules further reacts in the burning process to an average of 3.87e-01.

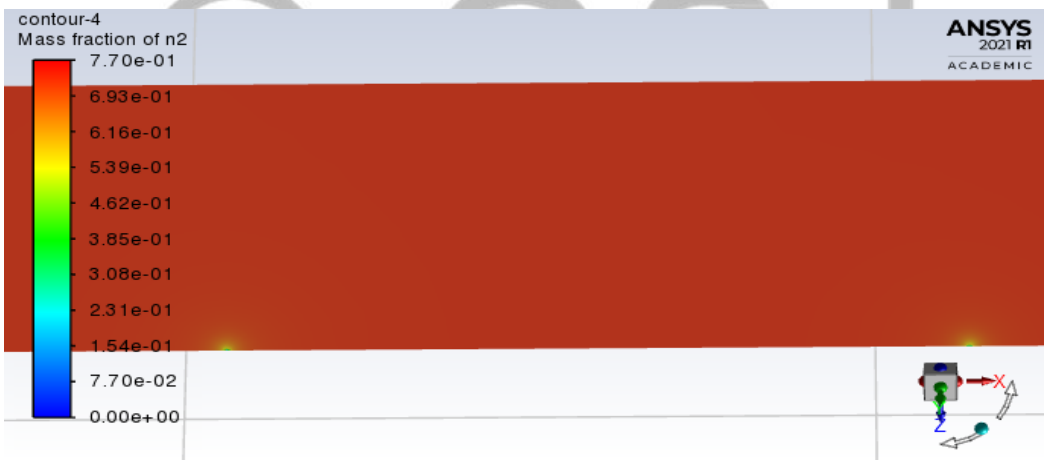

Figure 12. Contours plot of Nitrogen Mass Fraction of dual GDI

At the start of combustion, the mass fraction of Nitrogen is at its peak of 7.70e-01. As the flame propagates into the unburnt mixture, the Nitrogen molecules further reacts in the burning process to an average of 3.85e-01. The burning continues until there is no more nitrogen in the combustion chamber.

3.3 Comparison of mass fractions of Nitrogen N_2 in Single DI engine at early and late injection modes

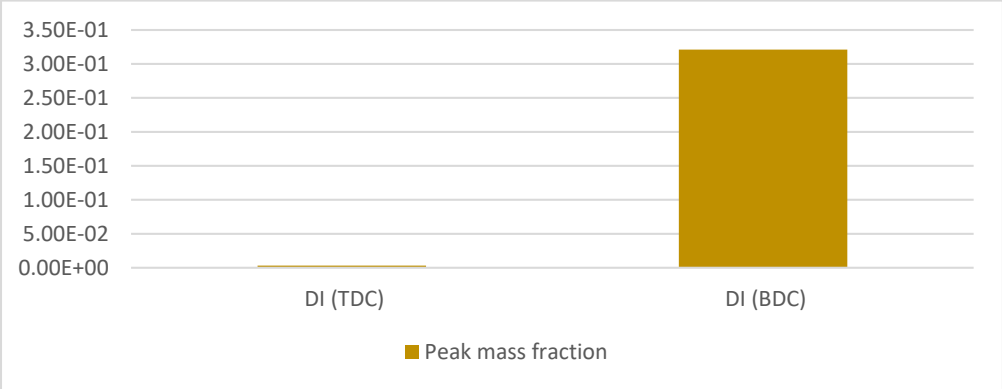

Figure 13. Mass fraction of Nitrogen of single GDI Engine operating modes

At the end of the combustion in the early injection mode, the mass fraction of nitrogen in the combustion chamber is 3.09e-03 as against 3.21e-01 in the case of late injection. This indicates that a little more nitrogen is used in combustion when the engine operates at early injection mode to the disadvantage of NOx formation than in the late injection modes of the single GDI engine.

3.4 Comparison of mass fractions of Nitrogen (N_2) in Dual DI engine at early and late injection modes

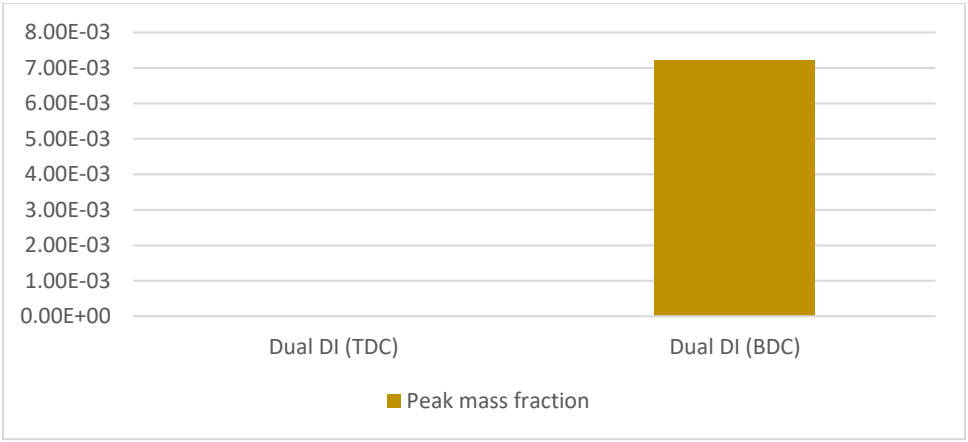

Figure 14. Mass fraction of Nitrogen of dual GDI Engine operating modes

At the end of the combustion in the early injection mode, the mass fraction of nitrogen in the combustion chamber is 0.00e+00 as against 7.21e-03 in the case of late injection. This indicates that all the nitrogen is used in combustion when the engine operates at early injection mode to the disadvantage of NOx formation than in the late injection modes of the dual GDI engine.

3.5 NOx Production at Late injection mode (piston at BDC)

Figure 15. Contours plot of NOx Mass Fraction—Prompt and Thermal NOx Formation of single GDI

The peak concentration of NOx is located in a region of high temperature where oxygen and nitrogen are available. The high concentration area has the highest mass fraction of NOx of 7.66e-34. The moderate temperature, oxygen and nitrogen concentrated area has an average mass fraction of 3.83e-34. The region of low temperature with lower oxygen and nitrogen has no mass fraction of NOx formed there and records 0.00e+00.
With the mass fraction of 7.66e-34, the Mass-Weighted Average shows that the exiting NOx mass fraction through the exhaust is 0.0

Figure 16. Contours plot of NOx Mass Fraction—Prompt and Thermal NOx Formation of dual GDI

The peak concentration of NOx is located in a region of high temperature where oxygen and nitrogen are available. The high concentration area has the highest mass fraction of NOx of 7.48e-28. The moderate temperature, oxygen and nitrogen concentrated area has an average mass fraction of 3.74e-28. The region of low temperature with lower oxygen and nitrogen has no mass fraction of NOx formed there and records 0.00e+00. With the mass fraction of 7.48e-28, the Mass-Weighted Average shows that the exiting NOx mass fraction through the exhaust is 0.0**.**

3.6 NOx Production at Early injection mode (piston at TDC)

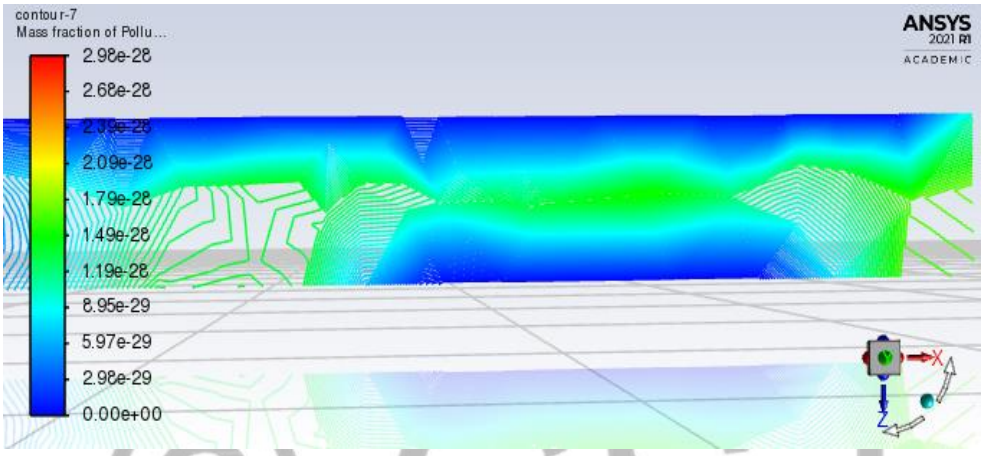

Figure 17. Contours plot of NOx Mass Fraction—Prompt and Thermal NOx Formation of single GDI

The peak concentration of NOx is located in a region of high temperature where oxygen and nitrogen are available. The high concentration area has the highest mass fraction of NOx of 2.98e-28. The moderate temperature, oxygen and nitrogen concentrated area has an average mass fraction of 1.49e-28. The region of low temperature with lower oxygen and nitrogen has no mass fraction of NOx formed there and records 0.00e+00. With the mass fraction of 2.98e-28, the Mass-Weighted Average shows that the exiting NOx mass fraction through the exhaust is 0.0

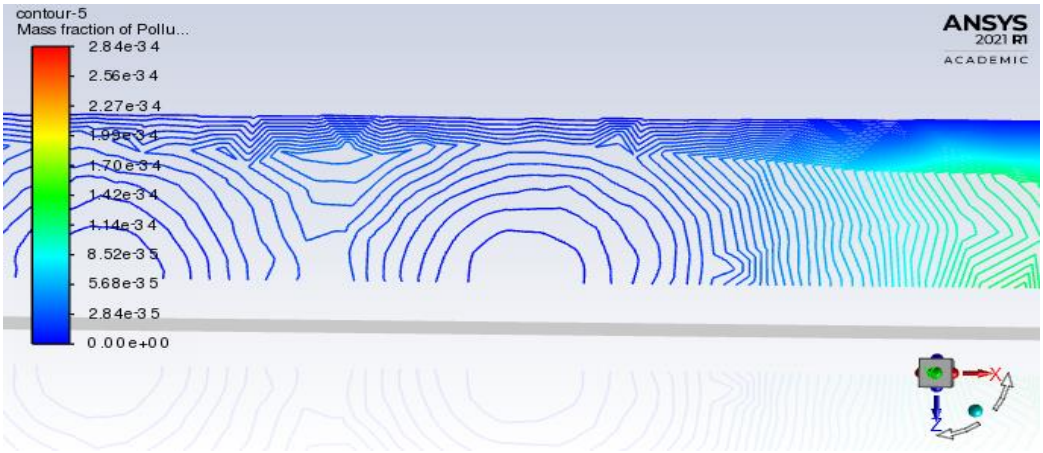

Figure 18. Contours plot of NOx Mass Fraction—Prompt and Thermal NOx Formation of dual GDI

The peak concentration of NOx is located in a region of high temperature where oxygen and nitrogen are available. The high concentration area has the highest mass fraction of NOx of 2.84e-34. The moderate temperature, oxygen and nitrogen concentrated area has an average mass fraction of 1.42e-34. The region of low temperature with lower oxygen and nitrogen has no mass fraction of NOx formed there and records 0.00e+00. With the mass fraction of 2.84e-34, the Mass-Weighted Average shows that the exiting NOx mass fraction through the exhaust is 0.0

3.7 Comparison of NOx mass fractions of single DI engines at early and late injection modes

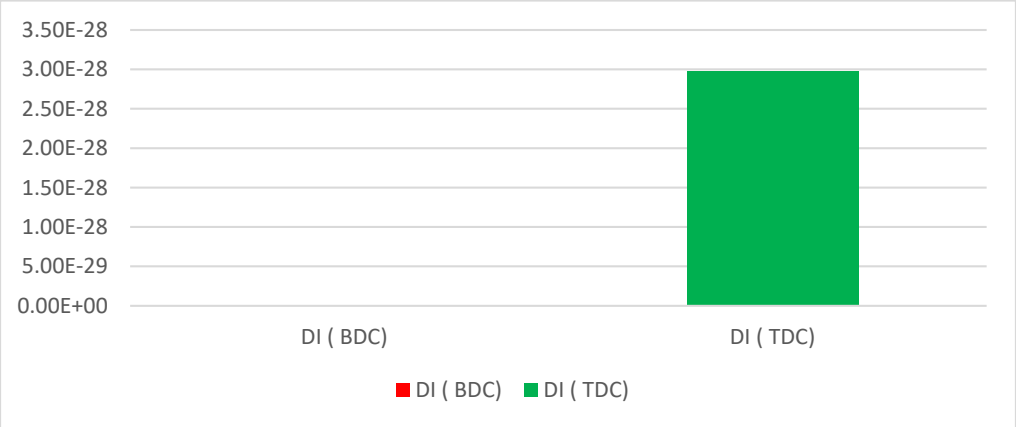

Figure 19: Mass fraction of NOx of single GDI Engine injection modes

From Fig 19, the formation of NOx in the single DI engine that injects fuel early is as high as 2.98e-28. On the other hand, the formation of NOx when the fuel is injected late in the single DI engine is 7.66e-34 which is far lower. In sum, when fuel-air mixture is injected late into the single DI engine, NOx formation is much improved as compared to early injection of fuel. The results for the single GDI engine varies from the results of Zheng et al. (2007) that homogenous charge reduces NO_x production in the single GDI.

3.8 Comparison of NOx mass fractions of dual DI engines at early and late injection modes

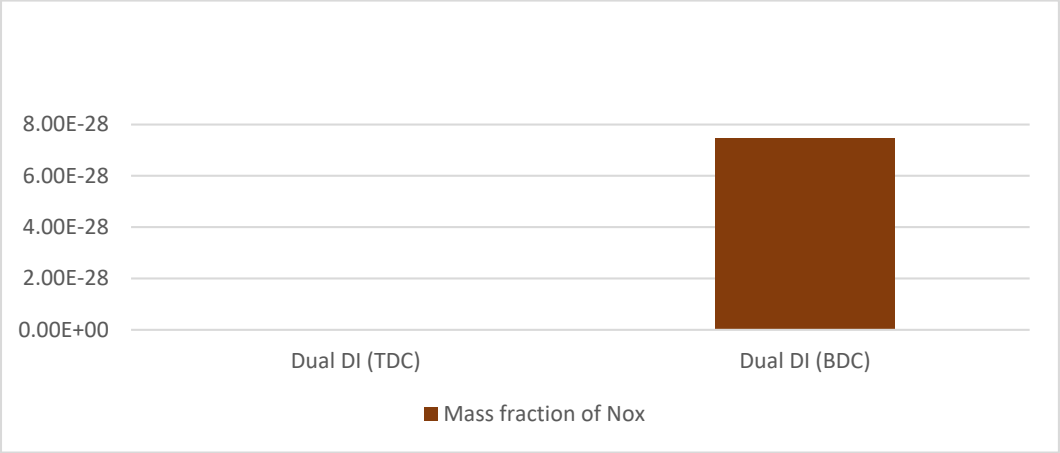

Figure 20: Mass fraction of NOx of dual GDI Engine injection modes

From Fig. 20, the formation of NOx in the dual DI engine that injects fuel late is as high as 7.48e-28. On the other hand, the formation of NOx when the fuel is injected early in the dual DI engine is 2.84e-34 which is far lower. In sum, when fuel-air mixture is injected early into the dual DI engine, NOx formation is by far improved than in the late fuel injection mode. This results agrees with the findings of Zheng et al. (2007) that early injection mode promises the reduction of NOx.

4.0 CONCLUSION

Late injection for stratified charge could realize Gasoline Direct Injection (GDI) engine's full potential in terms of fuel economy and emissions. Current study shows that lean mixture creation in the combustion chamber causes misfire, hydrocarbon and NOx emissions potentially weakening the engine's advantage over the port fuel injection (PFI) engines. This work explores the impact of dual direct injection on NOx formation in a GDI engine at early injection mode. 2021 ANSYS Design modeler was used for the geometry design, meshing, and employed ANSYS Fluent for simulation, and numerical analysis

However, it is evident from the results that N2 content and its corresponding NOx production in the dual direct injection engine is much lower during early injection modes as compared to when same is injected late. Dual direct injection appears to amplify the fuel's evaporative and cooling effect to mitigate NOx production.

REFERENCES

Anenberg, S., Miller, J., Henze, D., & Minjares, R. (2019). A global snapshot of the air pollution-related health impacts of transportation sector emissions in 2010 and 2015. *International Council on Clean Transportation*, 55. https://www.theicct.org/sites/default/files/publications/Global_health_impacts_transport_emissions_2010-2015_20190226.pdf

Awad, O. I., Ma, X., Kamil, M., Ali, O. M., Zhang, Z., & Shuai, S. (2020). Particulate emissions from gasoline direct injection engines: A review of how current emission regulations are being met by automobile manufacturers. *Science of the Total Environment*, *718*, 137302. https://doi.org/10.1016/j.scitotenv.2020.137302

Baidoo Philip (2020) the comparative study of the sway of effect pulse energies of pathways on AHSS-DP 350/600 and simulation. (J) Determinations in Nanomedicine & Nanotechnology (DNN), published; 2020, volume 1, Issue 5. (1(5). DNN.000525.2020)

Franchini, M., & Mannucci, P. M. (2015). Impact on human health of climate changes. *European Journal of Internal Medicine*, *26*(1), 1–5. https://doi.org/10.1016/j.ejim.2014.12.008

Kalghatgi, G. (2019). Development of Fuel / Engine Systems — The Way Forward to Sustainable Transport. *Engineering*, *5*(3), 510–518. https://doi.org/10.1016/j.eng.2019.01.009

Price, P., Twiney, B., Stone, R., Kar, K., & Walmsley, H. (2007). Particulate and hydrocarbon emissions from a spray guided direct injection spark ignition engine with oxygenate fuel blends. *SAE Technical Papers*, *724*, 776–790. https://doi.org/10.4271/2007-01-0472

Tekper, Isaac, Joseph Kwame Lewballah, James Kwasi Quaisie, Fred Joseph Komla Adzabe, Emmanuel Yeboah Osei, Emmanuel Asamoah, Philip Baidoo, and Andrews Danquah. "An Investigation into the Comparisons of Exhaust Emissions through Catalytic Converters Installed on a Kia Sportage Lx (Exhaust System)."(2020).

Zheng, M., Tan, Y., Mulenga, M. C., & Wang, M. (2007). Thermal efficiency analyses of diesel low temperature combustion cycles. *SAE Technical Papers*, *724*. https://doi.org/10.4271/2007-01-4019